Egypt. J. Chem. **Vol. 64,** No. 5 pp. 2509 - 2515 (2021)

Egyptian Journal of Chemistry

http://ejchem.journals.ekb.eg/

Synthesis and characterization of γ-Al_2O_3 and α-Al_2O_3 nanoparticles using a facile, inexpensive auto-combustion approach

Magdy I. Kandil[1], Hossam S. Jahin[2], Hassan A. Dessouki[1], Mostafa Y. Nassar[1]*

1Chemistry Department, Faculty of Science, Benha University, Benha 13815, Egypt

2Central Laboratory for Environmental Quality Monitoring (CLEQM), National Water Research Center (NWRC), Cairo, Egypt

Abstract

In the present work, we have developed a facile, inexpensive, auto-combustion method for the synthesis of γ-Al2O3 and α-Al2O3 nanoparticles. This was performed by employing aluminum nitrate as an oxidant and glycine as a fuel. The γ-Al2O3 and α-Al2O3 nanoparticles were obtained by calcination of the combusted products at 800 °C for 2 h and at 1000 °C for 1 h, respectively. The generated alumina nanoparticles were characterized by using X-ray diffraction (XRD), Fourier transform infrared spectroscopy (FT-IR), field-emission scanning electron microscope (FE-SEM), high-resolution transmission electron microscope (HRTEM), and thermal analyses (TG and DTA). The average crystallite sizes of γ-Al2O3 and α-Al2O3 nanoparticles were estimated to be 5.8 nm and 15 nm, respectively. The TEM results revealed that the prepared alumina nanostructures were of low agglomeration degree. The proposed method exhibited that the phases of the produced alumina nanoparticles could be carefully tuned by the adapted experimental conditions.
Keywords: γ-Al_2O_3 and α-Al_2O_3 nanoparticles; auto-combustion synthesis; Glycine fuel, characterization.

1. Introduction

Nanoparticles have unique characteristics compared to bulk materials; therefore, various research groups have devoted their effort to preparing of nanoparticles and using them in different applications [1-4]. Metal oxide nanoparticles have good stability, low poisonousness, and selectivity linked with organic substances [5-10]. They showed remarkable applications in catalysis, sensor devices, drug delivery, semiconductor materials, water treatment, and solid oxide fuels [7-12]. Among these metal oxides, Al_2O_3 nanoparticles are one of the nanostructures that have aroused keen interests of the materials science researchers owing to their wide applications such as wear protection, automotive emission control, hydrogenation, metallurgy, refractories, and catalysis in petroleum refining [13-15]. These various applications of alumina are due to its interesting characteristics including high catalytic surface activity, good optical activity, high corrosion resistance, and high surface area [16]. Furthermore, because of hardness, non-volatility, and resistance to oxidation and rust, as well as high melting points of aluminum oxides, they were used in ceramics [17-19]. Owing to their hollow porous microspheres, hierarchical architecture, and arranged mesoporous structure, aluminum oxides were also applied as adsorbents [20] for the removal of some organic compounds from aqueous media [21, 22], cosmetic fillers [23], polishing and packaging materials [24], and thermal conductivity enhancers [25].

Furthermore, aluminum oxide is an amphoteric oxide and exists in various polymorphs such as gamma (ɣ-), delta (δ-), theta (ɵ-), rho (ρ-), eta (η-), kappa (ƙ-) and chi (χ)-alumina, in addition to its stable phase (alpha (α)-alumina, corundum) [26]. Among them, alpha- and gamma-alumina have attracted a significant attention of the research groups based on their unique characteristics; therefore, both polymorphs have various applications as mentioned previously [13-16]. It is worth mentioning that corundum (α-alumina) is the most

*Corresponding authors: E-mail address: m_y_nassar@yahoo.com , m_y_nassar@fsc.bu.edu.eg (M.Y. Nassar).
Receive Date: 06 February 2021, Accept Date: 15 February 2021
DOI: 10.21608/EJCHEM.2021.61793.3330

thermodynamically stable and desirable polymorph of alumina. It has also high mechanical properties, chemical stabilities, and temperature resistance [15]. Consequently, synthesis of ɣ- and α-alumina nanoparticles is of great interest. Aluminum oxide nanoparticles were synthesized by different techniques such as hydrothermal synthesis [27], plasma synthesis [28], freeze-drying of sulfate solutions [29], the sol-gel method [30, 31], laser ablation [32], controlled hydrolysis of metal alkoxide [33], and precipitation [34], precipitation and sol-gel process followed by calcination [35, 36], sputtering [37], electrochemical [38], mechanical milling [39], pyrolysis [40], homogenous precipitation followed by calcination [41], and metal organic chemical vapor deposition [42]. However, limitations of these approaches, for both ɣ- and α-alumina nanoparticles, are of great concerns such as long reaction time, uncontrolled particle size, a high-temperature requirement, and use of expensive and toxic organic solvents. Besides, the synthesized ɣ-alumina nanoparticles sill experience some drawbacks such as non-dispersive particles and large particle sizes [43]. Therefore, it was notably essential to develop an inexpensive, facile, synthetic method to synthesize both ɣ- and α-alumina nanoparticles at lower temperatures.

In this study, we have developed a facile, inexpensive approach for gamma- and alpha-Al2O3 nanoparticles via an auto-combustion method employing aluminum nitrate as oxidant and glycine fuel as a reductant. The synthesized nanostructures were characterized by X-ray diffraction (XRD), Fourier transforms infrared spectroscopy (FTIR), field-emission scanning electron microscope (FE-SEM), high-resolution transmission electron microscope (HR-TEM), and thermogravimetric analysis (TGA).

2. Materials and Methods

2.1 Chemicals and Reagents

All materials and reagents in the current study were used as received without further purification since they were of analytical grade. Aluminum nitrate nonahydrate (Al (NO3)3.9H2O) was supplied by Oxford Lab. Fine Chem. LLP, India. Glycine (NH2CH2COOH) was obtained from El-Nasr Pharmaceutical Chemicals Company (Adwic) Company, Egypt.

2.2 Preparation of gamma- and alpha-Al2O3 nanoparticles

Aluminum oxide nanoparticles were prepared by utilizing an auto-combustion in which glycine fuel was used as a reductant (F), and aluminum nitrate was used as an oxidant (O). In this procedure, the determined stoichiometry of the employed redox mixture for the current combustion process was based on that the equivalence ratio, Φc, should be unity (i.e. Φc= (F/O)=1) to maximize the energy which was released from the combustion procedure. Where (O) is the total oxidizing valence of the oxidizer (i.e. aluminum nitrate) and (F) the total reducing valence of the glycine fuel [10, 44, 45]. In a typical preparation procedure: aluminum nitrate (Al (NO3)3.9H2O) (10 g, 26.67 mmol) and glycine fuel (NH2CH2COOH) (3.34 g, 44.54 mmol) were mixed and dissolved in 75 mL distilled water. The reaction blend was stirred at room temperature for ca. 15 min until a homogenous solution was obtained. The solution was then heated at ca. 80 ºC under constant stirring for 60 min until it gave a viscous liquid. Afterward, the temperature of the reaction blend was increased to ca. 350 °C, while the entire combustion was performed in ca. 10 min. During this, the reaction mixture underwent swelling and auto-ignition with a rapid evolution of a large volume of gases producing voluminous powders. The burned materials were ground and calcined for 2 h at 800 and for 1 h at 1000 °C to produce gamma- and alpha-Al2O3 nanoparticles, respectively. The schematic flowchart of the applied synthesis process is shown in (Scheme 1).

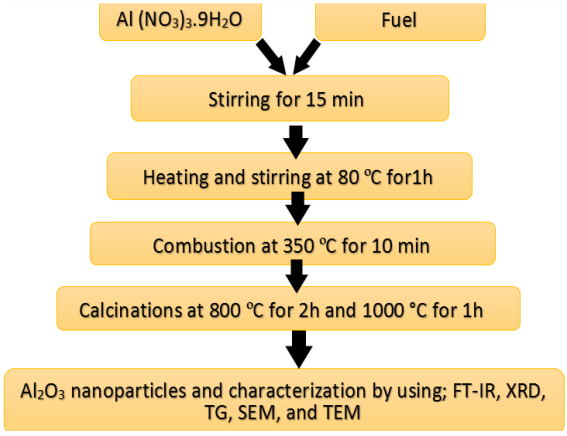

Scheme 1. Flowchart for the preparation procedure of Al_2O_3 nanoparticles by an auto-combustion method.

Characterization

The phase structure and purity of the as-prepared materials were investigated by using an X-ray diffractometer (Bruker, model D8 Advance) with Cu/K_α radiation (λ= 1.5418˚A) (Metallurgical Development Research Center, Cairo, Egypt). Surface morphology of the products were examined by using a field-emission scanning electron microscope (FE-SEM; model QUANTA-FEG-250) (Desert Research Center, Cairo,Egypt). The microstructures of the products were studies by suing a high-resolution transmission electron microscope ((JEOL; model 1200 EX) at an electron voltage of 80 kV (National Research Centre, Cairo, Egypt). The chemical structure of the products was further examined using FT-IR spectra measured on an FT-IR spectrometer (Thermo Scientific, model Nicolet iS10) in the frequency range of 400–4000 cm^{-1}, Chemistry Administration, Ministry of Trade and Industry, Cairo, Egypt. The thermal behavior of as-prepared powder was investigated by using thermal gravimetric analysis (TGA) and differential thermal analysis (DTA) (Shimadzu; model TA-60WS), Microanalytical Center, Cairo University, Cairo, Egypt. The thermal analysis was performed at heating rate of 10 °C/min under nitrogen gas atmosphere and the sample was heated from room temperature until 1000 °C.

3. Results and Discussion

The applied solution auto-combustion process is based on applying the thermochemical concepts of propellant chemistry [10, 44, 45]. Stoichiometric compositions of the mixtures (oxidant – reductant) for the combustion approach were calculated based on that the total oxidizing (O) and reducing (F) valences of the oxidant (aluminum nitrate) and reductant or fuel (glycine) so as to obtain the equivalence ratio (ϕ_c) equal unity (**i.e. ϕ_c = (oxidant/fuel) = 1**). This approach was utilized in the current research to prepare gamma- and alpha-aluminium oxide nanoparticles. As such glycine was used as a fuel and chelating agent for the aluminum element of the $Al(NO_3)_3$, which oxidized the fuel at high temperature at the same time. This procedure results in release of high energy, which is sufficient for producing Al_2O_3 nanoparticles. The suggested combustion reaction between aluminum nitrate and glycine to produce Al_2O_3 nanoparticles can be expressed as given in Eq (1).

$$6Al(NO_3)_3.9H_2O(aq) + 10C_2H_5NO_2(aq) \longrightarrow 3Al_2O_3(s) + 27N_2(g) + 20CO_2(g) + 79H_2O(g) \quad \text{Eq(1)}$$

The aforementioned combustion reaction gives rise to producing Al_2O_3 nanoparticles as well as emitting some gases such as CO_2, H_2O, and N_2, which result in high porosity of the products prepared using this approach. The burnt alumina samples were then calcined at 800 and 1000 ºC to generate the target gamma- and alpha-Al_2O_3 nanoparticles. The products were identified by using different techniques like XRD, FT-IR, TGA/DTA, SEM, and TEM analysis, as will be shortly mentioned.

3.1. X-ray diffraction (XRD) study

The XRD patterns of the burnt sample and the products calcined at 800 ºC for 2h and 1000 °C for 1h, are presented in (**Fig. 1)**. It was observed that the burnt sample has low crystallinity since Fig. 1(a) displayed only two broad peaks at 2θ = 45.9° and 66.9° corresponding to formation of γ-Al_2O_3 nanoparticles, (JPCDS card number: 10-0425) [46], directly after the combustion process. However, γ-Al_2O_3 product was impure for two reasons; (1) its grey color indicating the presence of much carbon content in the burnt sample, low crystallinity of the burnt product, which may contain other impurities with amorphous nature. Therefore, the crystallinity of this sample was enhanced by its calcination at the burnt sample 800 ºC for 2h. As expected, this calcination step gave rise to pure γ-Al_2O_3 product with significant crystallinity. The diffraction peaks of the respective XRD pattern (Fig. 1(b)) appeared at 2θ of 31.10º, 37.44º, 39.67º, 45.96º, 61.00º, and 66.97º could be matched well to the (220), (311), (222), (400), (511), and (440) crystal planes, respectively, of cubic γ-Al_2O_3 (JPCDS card number: 10-0425) [46]. However, the appearance of diffraction peak at 2θ of 33.44 º can be attributed to the transformation of tiny amount of γ-Al_2O_3 phase into θ-Al_2O_3 phase [15].

In addition, further calcination of the alumina product at 1000 ºC for 1h generated pure α-Al_2O_3 phase with significant crystallinity, as it is clearly seen from the XRD pattern (Fig. 1(c)) of this calcined alumina product. This XRD pattern displayed reflections at 2θ of 25.62º, 35.2º, 43.46º, 52.71º, 57.67º, and 66.59º which are matched-well with the (012), (104), (113), (024), (116), and (214) crystal planes, respectively, of rhombohedral α-Al_2O_3 phase (JPCDS card number: 46-1212) [47]. No other diffraction peaks have been detected for other impurities nor other alumina phases. The average crystallite sizes (D, nm) of the as-prepared alumina nanoparticles were determined using the Debye-Sherrer formula (2) [48]:

$$D=0.9\lambda/\beta\cos(\theta_B) \quad \text{Eq. (2)}$$

Where, **0.9** is Scherrer's constant, **β** is the full width at half maximum (FWHM) of the diffraction peak, **λ** (1.5406 A˚) is the wavelength of X-ray radiation, and θ_B the Bragg diffraction angle. The estimated average crystallite sizes of γ-Al_2O_3

and α-Al_2O_3 nanoparticles were found to be 5.8 and 15 nm, respectively. These values are smaller than reported by other research groups [41, 49].

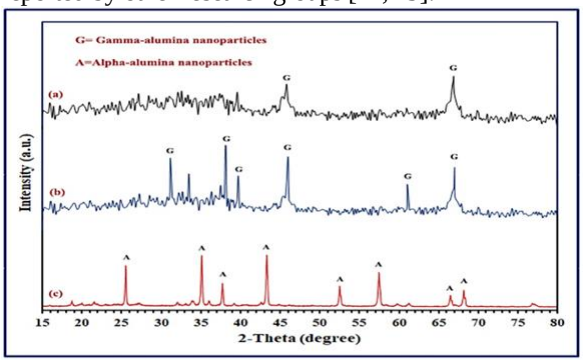

Fig. 1. XRD patterns of the combusted (a) and the calcined alumina products at 800 °C (b), and at 1000 °C (c).

3.2. FT-IR study

The chemical structures of the as-synthesized γ-Al_2O_3 and α-Al_2O_3 nanoparticles were inspected by using FT-IR spectroscopy, as depicted in Fig. 2. The vibration bands appeared at around 1641 and 3478 cm^{-1} for both FT-IR spectra could be corresponded to bending and stretching vibrations, respectively, of the adsorbed water molecules [3, 4]. Fig. 2(a) displayed two broad vibrational bands at 552 and 842 cm^{-1}, which can be assigned to Al–O stretching vibrations in an octahedral coordination (AlO_6) and a tetrahedral coordination (AlO_4) sites, respectively. These two bands are characteristics for γ-Al_2O_3 and these results are in good agreement with the XRD results and the published data [41, 50]. On the other hand, calcination of the alumina sample at 1000 °C for 1h gave rise to FT-IR spectrum shown in Fig. 2(b). This spectrum revealed vibrational bands at ca. 639.3, 588.19, 495.62, and 449.34 cm^{-1}, which can be attributed to α-Al_2O_3 nanoparticles [51]. These results are also compatible with the XRD data. Besides, both FT-IR spectra exhibited weak vibrational bands abound 1100 cm^{-1}, which may correspond to Al-O-H bonds [52]. Both This is a good agree with XRD results.

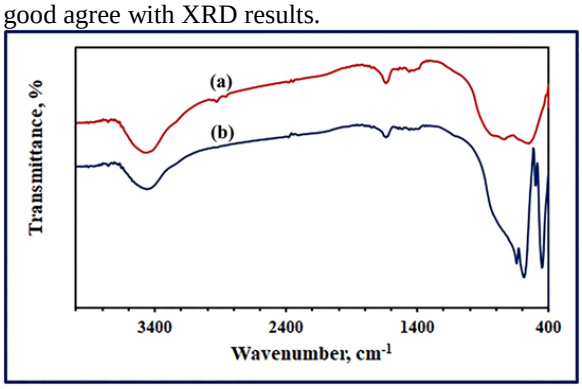

Fig. 2. FT-IR spectra of γ-Al_2O_3 (a) and α-Al_2O_3 (b) nanoparticles.

3.3. Thermal analysis study

Thermal behavior of the combusted sample was investigated using TG and DTA analysis, as displayed in Fig. 3. The TG curve of the combusted sample revealed four regions of mass losses. The first decomposition step (mass loss of 4.05%) observed in the temperature range 60 – 220 °C might be attributed to the dehydration of residual water content absorbed on the surface of the combusted sample. The second decomposition step (mass loss of 2.52%) appeared within a temperature range of 220-563 °C is probably due to dual decomposition of carbon content dehydration of Al-OH groups forming γ-Al_2O_3. This TG curve showed also a small third degradation step (mass loss of 0.40%) may be assigned to the decomposition of some organic content and dehydration of the remaining Al-OH groups forming γ-Al_2O_3. The last mass loss appeared in the temperature range of 660-860 °C, which may correspond to the decomposition of of the remaining carbon residue leaving behind pure γ-Al_2O_3, and this step is accompanied by mass loss of 5.0%. Then the mass of the sample remained constant after 860 °C. Moreover, Derivative thermogravimetric curve (DTG; Fig. 3) confirmed the TG data by revealing clearly the first, third and fourth steps at ca. 100, 575, and 790 °C, respectively. Differential thermal analysis (DTA) curve supported the results gained from TG data. The DTA curved exhibited two strong endothermic peaks at 173 and 870 °C, which are simultaneously parallel to the first and fourth steps in the TG curve. These are probably, as previously mentioned, due to the elimination of adsorbed water molecules and decomposition of the remaining carbon content. Notably, the second and third decomposition steps in the TG curve were merged in the DTA curve into one broad step centered at around 520 °C.

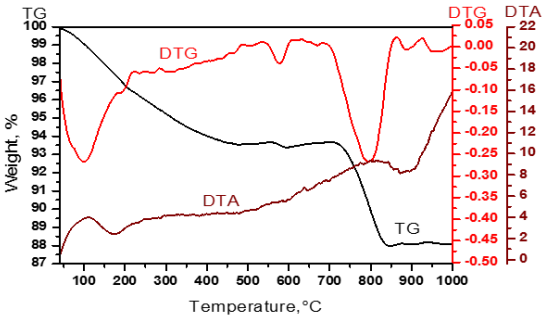

Fig. 3. TG, DTG, and DTA curves of the combusted sample.

3.4. Morphological investigation

Morphological characteristics of α-Al_2O_3 nanoparticles calcined at 1000 °C for 1h were investigated by utilizing FE-SEM and TEM

techniques, as displayed in Fig. 4(a,b). It is clearly seen from FE-SEM image (Fig. 4(a)) that the α-Al_2O_3 product is composed of agglomeration of irregular and leave-like morphologies. The TEM image of the α-Al_2O_3 product (Fig. 4(b)) revealed that the alumina product consists of hexagonal and irregular particles of an average particle size of 16.2 nm. Fig. 4(b) also showed that the α-alumina product is not totally agglomerated and somewhat dispersed. In addition, the HR-TEM image (Fig. 4(c)) of the alumina product calcined at 1000 °C obviously revealed fringes, which are oriented in various directions (planed with circles) corresponding to the different planes. These results also confirms the polycrystalline nature of α-Al_2O_3 nanoparticles, which are in consistent with the published results.

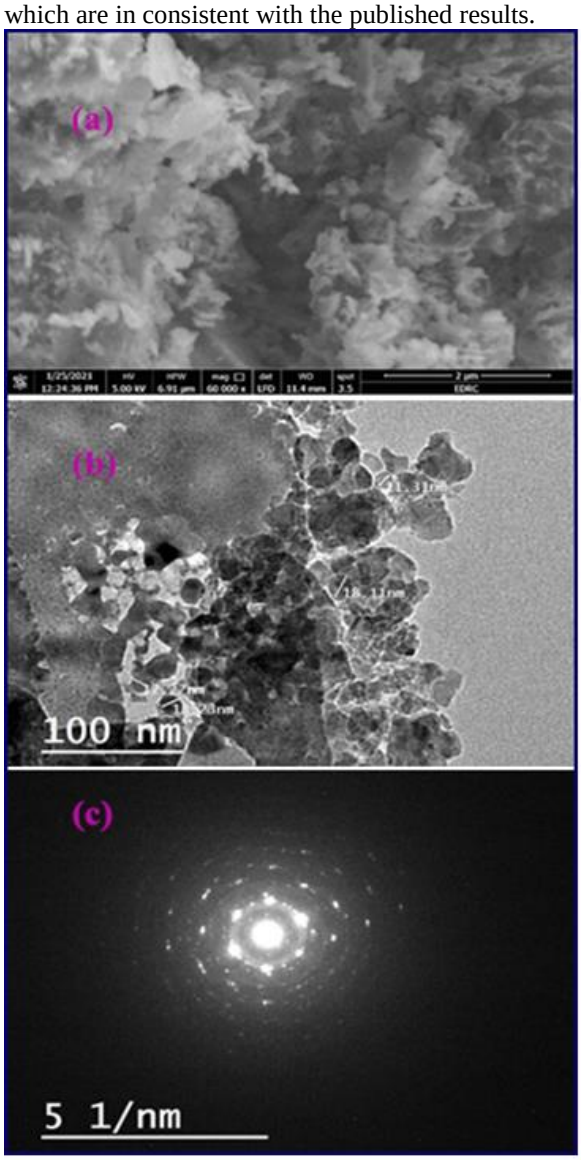

Fig. 5 FE-SEM image (a), TEM images (b), and HRTEM fast Fourier transform (FTT) (c) of the as-prepared α-Al_2O_3 nanoparticles.

4. Conclusions

In conclusion, γ-Al_2O_3 and α-Al_2O_3 nanostructures have been prepared by using a facile, inexpensive, economical auto-combustion approach. In this method aluminum nitrate and glycine fuel were used as an oxidant and a reductant, respectively. Controlling the calcination temperature tuned the produced alumina nanoparticles. Lower calcination temperature generated γ-Al_2O_3 nanoparticles while higher calcination temperature produced α-Al_2O_3. By adapting this method, the average crystallite sizes were 5.8 and 15 nm, respectively, for γ-Al_2O_3 and α-Al_2O_3 nanoparticles. The prepared alumina nanoparticles were of low degree of agglomeration. Accordingly, the adapted method can be proposed for synthesis of various alumina phases, easily and economically.

References

[1] S. Chandra, A. Kumar, P.K. Tomar, Synthesis of Al nanoparticles: Transmission electron microscopy, thermal and spectral studies, Spectrochimica Acta Part A: Molecular and Biomolecular Spectroscopy 92 (2012) 392-397.

[2] W.-T. Liu, Nanoparticles and their biological and environmental applications, Journal of bioscience and bioengineering 102(1) (2006) 1-7.

[3] M.F. El-Berry, S.A. Sadeek, A.M. Abdalla, M.Y. Nassar, Microwave-assisted fabrication of copper nanoparticles utilizing different counter ions: An efficient photocatalyst for photocatalytic degradation of safranin dye from aqueous media, Materials Research Bulletin 133 (2021) 111048.

[4] M.M. Sobeih, M.F. El-Shahat, A. Osman, M.A. Zaid, M.Y. Nassar, Glauconite clay-functionalized chitosan nanocomposites for efficient adsorptive removal of fluoride ions from polluted aqueous solutions, RSC Advances 10(43) (2020) 25567-25585.

[5] N.A. Jasim, F.A. Al-Gasha'a, M.F. Al-Marjani, A.H. Al-Rahal, H.A. Abid, N.A. Al-Kadhmi, M. Jakaria, A.M. Rheima, ZnO nanoparticles inhibit growth and biofilm formation of vancomycin-resistant S. aureus (VRSA), Biocatalysis and Agricultural Biotechnology 29 (2020) 101745.

[6] A.H. Ismail, H.K. Al-Bairmani, Nano-synthesis, spectroscopic characterisation and antibacterial activity of some metal complexes derived from Theophylline, Egyptian Journal of Chemistry 63(12) (2020) 4951-4962.

[7] A.S. Abdel-Bary, D.A. Tolan, M.Y. Nassar, T. Taketsugu, A.M. El-Nahas, Chitosan, magnetite, silicon dioxide, and graphene oxide nanocomposites: Synthesis, characterization, efficiency as cisplatin drug delivery, and DFT calculations, International Journal of Biological Macromolecules 154 (2020) 621-633.

[8] M.Y. Nassar, I.S. Ahmed, M.A. Raya, A facile and tunable approach for synthesis of pure silica nanostructures from rice husk for the removal of ciprofloxacin drug from polluted aqueous solutions, Journal of Molecular Liquids 282 (2019) 251-263.
[9] M.Y. Nassar, I.S. Ahmed, H.S. Hendy, A facile one-pot hydrothermal synthesis of hematite (α-Fe2O3) nanostructures and cephalexin antibiotic sorptive removal from polluted aqueous media, Journal of Molecular Liquids 271 (2018) 844-856.
[10] M.Y. Nassar, T.Y. Mohamed, I.S. Ahmed, I. Samir, MgO nanostructure via a sol-gel combustion synthesis method using different fuels: An efficient nano-adsorbent for the removal of some anionic textile dyes, Journal of Molecular Liquids 225 (2017) 730-740.
[11] A.M. Rheima, D.H. Hussain, H.J. Abed, Fabrication of a new photo-sensitized solar cell using TiO2\ZnO Nanocomposite synthesized via a modified sol-gel Technique, IOP Conference Series: Materials Science and Engineering, IOP Publishing, 2020, p. 052036.
[12] A. Rheima, A. Anber, A. Shakir, A. Salah Hammed, S. Hameed, Novel method to synthesis nickel oxide nanoparticles for antibacterial activity, Iranian Journal of Physics Research 20(3) (2020) 51-55.
[13] S. Tabesh, F. Davar, M.R. Loghman-Estarki, Preparation of γ-Al2O3 nanoparticles using modified sol-gel method and its use for the adsorption of lead and cadmium ions, Journal of Alloys and Compounds 730 (2018) 441-449.
[14] Z. Zarnegar, Z. Shokrani, J. Safari, Asparagine functionalized Al2O3 nanoparticle as a superior heterogeneous organocatalyst in the synthesis of 2-aminothiazoles, Journal of Molecular Structure 1185 (2019) 143-152.
[15] P. Nayar, S. Waghmare, P. Singh, M. Najar, S. Puttewar, A. Agnihotri, Comparative study of phase transformation of Al2O3 nanoparticles prepared by chemical precipitation and sol-gel auto combustion methods, Materials Today: Proceedings 26 (2020) 122-125.
[16] L. Zhu, L. Liu, C. Sun, X. Zhang, L. Zhang, Z. Gao, G. Ye, H. Li, Low temperature synthesis of polyhedral α-Al2O3 nanoparticles through two different modes of planetary ball milling, Ceramics International 46(18, Part A) (2020) 28414-28421.
[17] B. Tang, J. Ge, L. Zhuo, G. Wang, J. Niu, Z. Shi, Y. Dong, A Facile and Controllable Synthesis of γ-Al2O3 Nanostructures without a Surfactant, European journal of inorganic chemistry 2005(21) (2005) 4366-4369.
[18] S. Zhou, M. Antonietti, M. Niederberger, Low-temperature synthesis of γ-alumina nanocrystals from aluminum acetylacetonate in nonaqueous media, Small 3(5) (2007) 763-767.
[19] B. Reddy, K. Das, S. Das, A review on the synthesis of in situ aluminum based composites by thermal, mechanical and mechanical–thermal activation of chemical reactions, Journal of Materials Science 42(22) (2007) 9366-9378.
[20] J. Tian, P. Tian, H. Pang, G. Ning, R.F. Bogale, H. Cheng, S. Shen, Fabrication synthesis of porous Al2O3 hollow microspheres and its superior adsorption performance for organic dye, Microporous and Mesoporous Materials 223 (2016) 27-34.
[21] A. Adak, M. Bandyopadhyay, A. Pal, Adsorption of anionic surfactant on alumina and reuse of the surfactant-modified alumina for the removal of crystal violet from aquatic environment, Journal of environmental science and health 40(1) (2005) 167-182.
[22] M.C. Patterson, N.D. Keilbart, L.W. Kiruri, C.A. Thibodeaux, S. Lomnicki, R.L. Kurtz, E. Poliakoff, B. Dellinger, P.T. Sprunger, EPFR formation from phenol adsorption on Al2O3 and TiO2: EPR and EELS studies, Chemical physics 422 (2013) 277-282.
[23] S.O. Alsharif, H.M. Akil, N.A.A. El-Aziz, Z.A.B. Ahmad, Influence of Al2O3 as filler loading on the fracture toughness of light-cured dental resin composites, Advanced Materials Research, Trans Tech Publ, 2013, pp. 227-231.
[24] R.K. Singh, K. Balasundaram, A.C. Arjunan, D. Singh, W. Bai, Chemical mechanical polishing of alumina, Google Patents, 2017.
[25] M.P. Beck, T. Sun, A.S. Teja, The thermal conductivity of alumina nanoparticles dispersed in ethylene glycol, Fluid Phase Equilibria 260(2) (2007) 275-278.
[26] M. Digne, P. Sautet, P. Raybaud, H. Toulhoat, E. Artacho, Structure and stability of aluminum hydroxides: a theoretical study, The Journal of Physical Chemistry B 106(20) (2002) 5155-5162.
[27] W.L. Suchanek, Hydrothermal synthesis of alpha alumina (α-Al2O3) powders: study of the processing variables and growth mechanisms, Journal of the American Ceramic Society 93(2) (2010) 399-412.
[28] P. Ananthapadmanabhan, K. Sreekumar, N. Venkatramani, P. Sinha, P.R. Taylor, Characterization of plasma-synthesized alumina, Journal of alloys and compounds 244(1-2) (1996) 70-74.
[29] M.I. Nieto, C. Tallon, R. Moreno, Synthesis of gamma-alumina nanoparticles by freeze drying,

Advances in Science and Technology, Trans Tech Publ, 2006, pp. 223-230.
[30] M. Nguefack, A.F. Popa, S. Rossignol, C. Kappenstein, Preparation of alumina through a sol–gel process. Synthesis, characterization, thermal evolution and model of intermediate boehmite, Physical Chemistry Chemical Physics 5(19) (2003) 4279-4289.
[31] R. Rogojan, E. Andronescu, C. Ghitulica, B.S. Vasile, Synthesis and characterization of alumina nano-powder obtained by sol-gel method, UPB Buletin Stiintific, Series B: Chemistry and Materials Science 73(2) (2011) 67-76.
[32] V. Piriyawong, V. Thongpool, P. Asanithi, P. Limsuwan, Preparation and characterization of alumina nanoparticles in deionized water using laser ablation technique, Journal of Nanomaterials 2012 (2012).
[33] T. Ogihara, H. Nakajima, T. Yanagawa, N. Ogata, K. Yoshida, N. Matsushita, Preparation of monodisperse, spherical alumina powders from alkoxides, Journal of the American Ceramic Society 74(9) (1991) 2263-2269.
[34] K. Inoue, M. Hama, Y. Kobayashi, Y. Yasuda, T. Morita, Low temperature synthesis of α-alumina with a seeding technique, International Scholarly Research Notices 2013 (2013).
[35] M. Shojaie-Bahaabad, E. Taheri-Nassaj, Economical synthesis of nano alumina powder using an aqueous sol–gel method, Materials Letters 62(19) (2008) 3364-3366.
[36] F. Mirjalili, M. Hasmaliza, L.C. Abdullah, Size-controlled synthesis of nano α-alumina particles through the sol–gel method, Ceramics International 36(4) (2010) 1253-1257.
[37] D.H. Trinh, M. Ottosson, M. Beckers, M. Collin, I. Reineck, L. Hultman, H. Högberg, Structural and mechanical characterisation of nanocomposite Al2O3-ZrO2 thin films grown by reactive dual radio-frequency magnetron sputtering", (2006).
[38] J. García-Mayorga, G. Urbano-Reyes, M. Veloz-Rodríguez, V. Reyes-Cruz, J. Cobos-Murcia, J. Hernández-Ávila, M. Pérez-Labra, Electrochemical preparation of precursor phases for obtaining alpha-alumina from aluminium scrap, Ceramics International 44(7) (2018) 7435-7441.
[39] C.B. Reid, J.S. Forrester, H.J. Goodshaw, E.H. Kisi, G.J. Suaning, A study in the mechanical milling of alumina powder, Ceramics International 34(6) (2008) 1551-1556.
[40] R.K. Pati, J.C. Ray, P. Pramanik, Synthesis of nanocrystalline α-alumina powder using triethanolamine, Journal of the American Ceramic Society 84(12) (2001) 2849-2852.
[41] J. Wang, D. Zhao, G. Zhou, C. Zhang, P. Zhang, X. Hou, Synthesis of nano-sized γ-Al2O3 with controllable size by simple homogeneous precipitation method, Materials Letters 279 (2020) 128476.
[42] H. Noda, K. Muramoto, H. Kim, Preparation of nano-structured ceramics using nanosized Al2O3 particles, Journal of Materials Science 38(9) (2003) 2043-2047.
[43] L. Zhu, S. Pu, K. Liu, T. Zhu, F. Lu, J. Li, Preparation and characterizations of porous γ-Al2O3 nanoparticles, Materials Letters 83 (2012) 73-75.
[44] S.R. Jain, K.C. Adiga, V.R. Pai Verneker, A new approach to thermochemical calculations of condensed fuel-oxidizer mixtures, Combustion and Flame 40 (1981) 71-79.
[45] M.Y. Nassar, I.S. Ahmed, I. Samir, A novel synthetic route for magnesium aluminate (MgAl2O4) nanoparticles using sol–gel auto combustion method and their photocatalytic properties, Spectrochimica Acta Part A: Molecular and Biomolecular Spectroscopy 131 (2014) 329-334.
[46] J. Yu, H. Bai, J. Wang, Z. Li, C. Jiao, Q. Liu, M. Zhang, L. Liu, Synthesis of alumina nanosheets via supercritical fluid technology with high uranyl adsorptive capacity, New Journal of Chemistry 37(2) (2013) 366-372.
[47] E.N. Maslen, V.A. Streltsov, N.R. Streltsova, N. Ishizawa, Y. Satow, Synchrotron X-ray study of the electron density in [alpha]-Al2O3, Acta Crystallographica Section B 49(6) (1993) 973-980.
[48] U. Holzwarth, N. Gibson, The Scherrer equation versus the'Debye-Scherrer equation', Nature nanotechnology 6(9) (2011) 534-534.
[49] A.A. Mohammed, Z.T. Khodair, A.A. Khadom, Preparation and investigation of the structural properties of α-Al2O3 nanoparticles using the sol-gel method, Chemical Data Collections 29 (2020) 100531.
[50] J. Gangwar, B.K. Gupta, P. Kumar, S.K. Tripathi, A.K. Srivastava, Time-resolved and photoluminescence spectroscopy of θ-Al2O3 nanowires for promising fast optical sensor applications, Dalton transactions 43(45) (2014) 17034-17043.
[51] A. Barker Jr, Infrared lattice vibrations and dielectric dispersion in corundum, Physical review 132(4) (1963) 1474.
[52] H. Özdemir, M.A. Faruk Öksüzömer, Synthesis of Al2O3, MgO and MgAl2O4 by solution combustion method and investigation of performances in partial oxidation of methane, Powder Technology 359 (2020) 107-117.